IEEE Access
Multidisciplinary | Rapid Review | Open Access Journal

Received February 21, 2019, accepted March 24, 2019, date of publication April 1, 2019, date of current version April 16, 2019.

Digital Object Identifier 10.1109/ACCESS.2019.2908451

Correction of Barrel Distortion in Fisheye Lens Images Using Image-Based Estimation of Distortion Parameters

MINJUNG LEE, HYUNGTAE KIM, (Student Member, IEEE), AND JOONKI PAIK, (Senior Member, IEEE)

Department of Image, Chung-Ang University, Seoul 06974, South Korea

Corresponding author: Joonki Paik (paikj@cau.ac.kr)

This work was supported in part by the Institute for Information and Communications Technology Planning and Evaluation(IITP) through the Korea Government (MSIT)—Development of global multi-target tracking and event prediction techniques based on real-time large-scale video analysis under Grant 2014-0-00077, and in part by the Institute for Information & Communications Technology Promotion(IITP) through the Korea Government (MSIT)—Intelligent Defense Boundary Surveillance Technology Using Collaborative Reinforced Learning of Embedded Edge Camera and Image Analysis under Grant 2017-0-00250.

ABSTRACT Images acquired by a fisheye lens camera contain geometric distortion that results in deformation of the object's shape. To correct the lens distortion, existing methods use prior information, such as calibration patterns or lens design specifications. However, the use of a calibration pattern works only when an input scene is a 2-D plane at a prespecified position. On the other hand, the lens design specifications can be understood only by optical experts. To solve these problems, we present a novel image-based algorithm that corrects the geometric distortion. The proposed algorithm consists of three stages: i) feature detection, ii) distortion parameter estimation, and iii) selection of the optimally corrected image out of multiple corrected candidates. The proposed method can automatically select the optimal amount of correction for a fisheye lens distortion by analyzing characteristics of the distorted image using neither prespecified lens design parameters nor calibration patterns. Furthermore, our method performs not only on-line correction by using facial landmark points, but also off-line correction described in subsection III-C. As a result, the proposed method can be applied to a virtual reality (VR) or augmented reality (AR) camera with two fisheye lenses in a field-of-view (FOV) of 195°, autonomous vehicle vision systems, wide-area visual surveillance systems, and unmanned aerial vehicle (UAV) cameras.

INDEX TERMS Lens distortion correction, fisheye lens, geometric distortion, facial landmark features, distortion parameter estimation.

I. INTRODUCTION

Recently, various vision systems have adopted a fisheye lens[1] to acquire an extended field of view (FoV) [1], [2]. This approach leverages the wide-angle lens to generate the contents of augmented reality (AR) or virtual reality (VR), and to improve the performance of intelligent robot vision systems [3]–[6]. Unfortunately, the fisheye lens has a geometrical distortions including tangential and barrel distortions. In this paper, we only consider the barrel distortion since the tangential distortion is made from the misalignment of a sensor and lens [7]. In addition, recent research on the lens distortion deals with the radial distortion without tangential distortion [8], [9]. The barrel distortion occurs in a space-variant manner along the radial direction, and the amount of distortion is proportional to the distance from the optical center [10], [11]. The eventual effect of the barrel distortion includes deformation of the shape of an object and transformation of a straight line into a curve. For that reason, fisheye lens-based vision systems need an appropriate method to correct the distortion [12].

Many researchers have tried to correct fisheye lens distortion. Major approaches to estimate the distortion model parameters are classified into three categories: i) geometric projection model-based, ii) calibration pattern-based, and iii) image-based or feature-based methods. The geometric projection model defines a relationship between the input undistorted scene and the output distorted image [13]. The geometric projection model-based correction method

The associate editor coordinating the review of this manuscript and approving it for publication was Peng Liu.

[1]The visual angle of a fisheye lens is close to or more than 180 degrees.

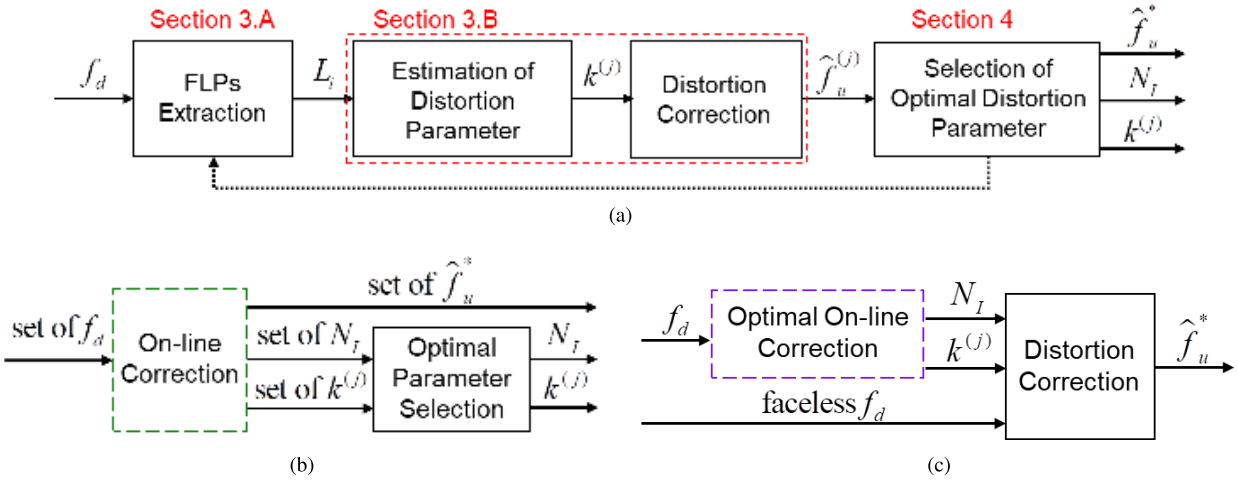

FIGURE 1. Block diagrams of the proposed image-based algorithm to correct the fisheye lens distortion: (a) on-line correction with an input containing facial features, (b) on-line correction with multiple images containing facial features, and (c) off-line correction using precalibration for a general input image without facial features. 'faceless f_d' represents an input image containing no faces.

requires the lens design specifications and the focal length. However, a perfect correction is not possible since the lens parameters are not available in many practical applications. The calibration pattern-based method uses *a priori* known pattern that is distorted by the lens [14]–[16]. These methods define the distortion ratio using the relationship between the ideal pattern image and its distorted version. The performance of the pattern-based correction method depends on the accuracy of an acquired pattern image.

For easier implementation of the pattern-based correction method, an image-based distortion parameter estimation method was proposed by Lee *et al.* [17]. Lee's method first trains the facial landmark points (FLPs) extracted in the undistorted image and then estimates the distortion parameter using the extracted FLPs. The accuracy of Lee's method depends on the number of training images containing meaningful features. An alternative method to estimate the distortion parameters was proposed by Cho *et al.* [18]. Cho's method uses the optical characteristics of the distortion, whose amount is proportional to the distance from the optical center along the radial direction. The major limitation of Cho's method is the manual off-line processing to obtain user-defined threshold values according to the size of an input image.

To solve these problems, this paper presents a novel image-based distortion parameter estimation method that selects the optimally corrected image using features in the input distorted image. The major contribution of the proposed research is twofold: i) both distortion parameter estimation and optimally corrected image selection processes require neither prespecified lens parameters nor special calibration patterns, and ii) both on-line and off-line corrections are possible.[2] Fig. 1 shows a block diagrams of the proposed algorithm for different application environments.

[2]If an input image contains facial features, the proposed method works on-line. Otherwise, an off-line precalibration data can be used.

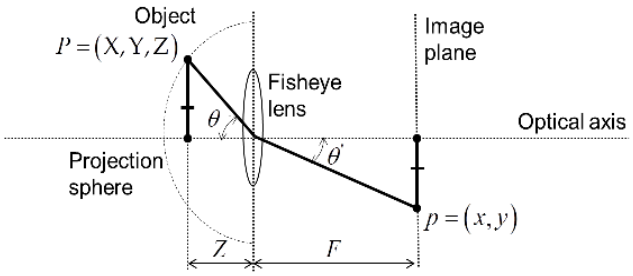

FIGURE 2. Fisheye lens projection model.

This paper is organized as follows. Section 2 summarizes the theoretical background. Section 3 describes the facial landmark feature extraction and distortion parameter estimation methods. Section 4 presents an automatic selection method for the optimally corrected image among multiple iterative solutions. After experimental results are given in section 5, section 6 concludes the paper. The convention of terminologies used in this paper is summarized in Table 3.

II. THEORETICAL BACKGROUND

A. PROJECTION SPHERE-BASED MODELS FOR FISHEYE LENS

The perspective projection is a theoretical foundation of most thin-lens camera systems, a wide-angle or fisheye lens camera does not follow the relationship because the projection between the object point P and the projected point p is a nonlinear function of the incidence angle of the object point ($\theta \neq \theta'$), as shown in Fig. 2.

The refracted ray by the fisheye lens makes a barrel distortion in the acquired image, in which an object shape is deformed in the radial direction. To understand the fisheye lens projection model, we can use a projection sphere. Fig. 3 intuitively demonstrates both perspective and fisheye lens projection models using the projection sphere with the same object and image plane. As shown in Fig. 3, the fisheye

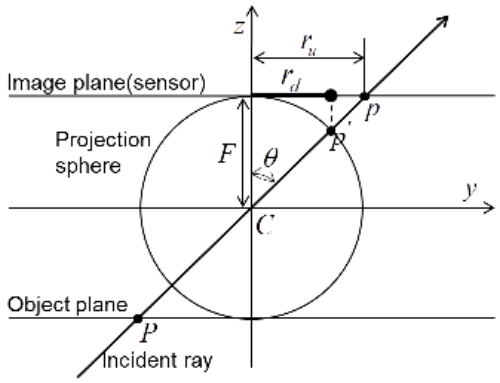

FIGURE 3. Orthographic projection model of fisheye lens imaging. A light ray starting from P on the object plane comes into the center C with the incident angle θ. If C is just a pinhole without a fisheye lens, its image is formed at p, whose radial distance is r_u, on the image plane. However, if the ray is refracted by the fisheye lens, its virtual image is formed at p' on the projection sphere, and its orthogonal projection onto the image plane determines the radial distance r_d.

lens projection point p' does not follow the perspective projection scheme. More specifically, the relationship between p and p' in Fig. 3 is spatially variant. There are four different projection models to describe the spatially variant relationship including: i) equidistant, ii) equisolid, iii) orthographic, and iv) stereographic models according to the projection types [13].

Each projection model provides a relationship between the radial distances of the undistorted and distorted points from the center, denoted as r_u and r_d, respectively. Because the angle of an incident ray θ uniquely determines r_u in the projection sphere, a function of the incident angle θ can define the projection mapping function that determines r_d. Projection mapping functions of the four models in Fig. 3 are defined as follows.

$$\begin{aligned} (a)Equidistant &: r_d = F\theta \\ (b)Equisolid &: r_d = 2F\sin(\theta/2) \\ (c)Orthographic &: r_d = F\sin\theta \\ (d)Stereographic &: r_d = 2F\tan(\theta/2) \end{aligned} \tag{1}$$

where F, θ, and r_d respectively represent the focal length, incident angle, and distance between the center and the projected point in the distorted image.

B. RATIONAL FUNCTION-BASED MODELS USING A CALIBRATION PATTERN

Although the projection sphere-based models provide an intuitive description of the projection, they cannot be applied to a lens whose field of view is larger than 180 °. To correct the geometric distortion due to a very wide-angle lens, a calibration pattern is used to generate the relationship between an ideal undistorted point and the distorted point. The pattern-based method characterizes the relationship between r_d/r_u versus r_u using a distortion curve as shown in Fig. 4.

The pattern-based method can generate an accurate distortion ratio only if there exist sufficiently many pairs of

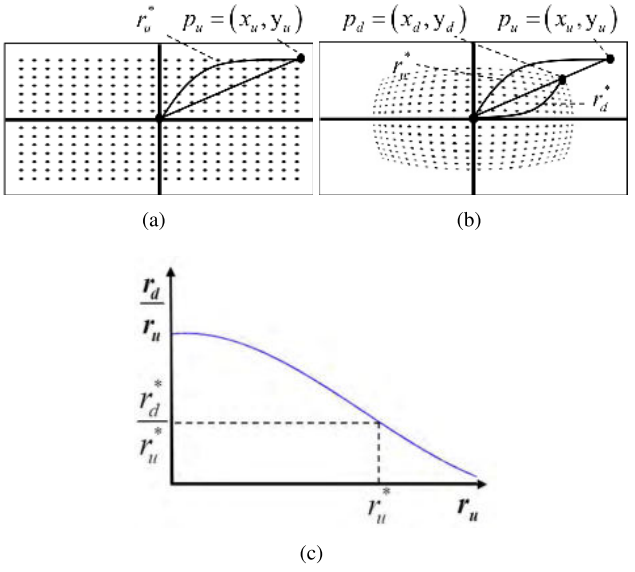

FIGURE 4. Estimation of the distortion parameters using a calibration pattern-based method: (a) a calibration pattern, (b) a projected pattern image by a fisheye lens, and (c) a distortion curve (r_d/r_u versus r_u).

undistorted and distorted points. Since points in the distorted image are distributed in a limited area as shown in Fig. 4(b), the distortion ratio over the entire image cannot be estimated.

To solve this problem, rational function-based distortion models were proposed in the literature [19]–[22]. Alemán-Flores *et al.* established the relationship between the distorted and undistorted points using a polynomial function as [22]

$$\begin{bmatrix} x_d - x_c \\ y_d - y_c \end{bmatrix} = L(r_u) \begin{bmatrix} x_u - x_c \\ y_u - y_c \end{bmatrix}, \tag{2}$$

for

$$L(r_u) = 1 + k_1 r_d^2 + k_2 r_d^4 + \cdots, \tag{3}$$

where (x_u, y_u), (x_d, y_d), and (x_c, y_c) respectively represent the coordinates of the undistorted point, distorted point, and image center, and

$$r_u = \sqrt{(x_u - x_c)^2 + (y_u - y_c)^2}. \tag{4}$$

In their original work, the undistorted point is represented as the distorted point divided by $L(r_u)$, which is called the division model as

$$\begin{bmatrix} x_u - x_c \\ y_u - y_c \end{bmatrix} = \frac{1}{L(r_u)} \begin{bmatrix} x_d - x_c \\ y_d - y_c \end{bmatrix}. \tag{5}$$

If we estimate the distortion parameters, $\{k_1, k_2, \ldots\}$, the distortion point can be computed from the undistorted point using (2).

In the rest of this paper, we use the distortion model given in (2) of the first order, that is $L(r_u) = 1 + k_1 r_d^2$, since we observed that the second-order or higher-order models result in only trivial improvement. Since the modeling of a fisheye lens is not the scope of this work, we do not further discuss about the analysis of the accuracy of different distortion models.

III. AUTOMATIC DISTORTION PARAMETER ESTIMATION IN A SINGLE DISTORTED IMAGE

This section presents an on-line automatic distortion correction algorithm based on facial features in the image without using a prior information. More specifically, we extract FLPs as the facial feature and estimate the distortion parameters using the extracted FLPs in a single distorted image. Since the distortion of a fisheye lens camera generally deforms local regions in different manners, the deformation-robust feature plays an important role in estimating accurate distortion parameters. A straightforward way to detect a general-shape object is image segmentation [23]. However, we present an efficient method to extract facial landmark points. Among various applications using facial features, eye-tracking is popular in the virtual reality field [24].

A. FACIAL LANDMARK POINTS (FLPS)

In the input distorted image, f_d, we first detect all faces and then extract a set of five FLPs from each face. Milborrow's method can accurately extract FLPs in the undistorted image using Stacked Trimmed Active Shape Model (STASM) only with the frontal face without occlusions [25]. To extract features from a non-frontal face possibly with a partial occlusion, we used the robust multi-task deep cascaded convolutional neural network (CNN) proposed by Zhang *et al.* [26].

Let N_F be the number of faces, and L_i, $i = 1, \ldots, N_F$, the i-th set of five FLP coordinates including the left eye (LE), right eye (RE), nose (N), left corner of the mouth (LM), and right corner of the mouth (RM). Let p^i_F, $F \in \{LE, RE, N, LM, RM\}$, be the five coordinates, then the i-th set of FLPs and its mean coordinates are respectively expressed as

$$\begin{aligned} L_i &= \{p^i_{LE}, p^i_{RE}, p^i_N, p^i_{LM}, p^i_{RM}\}, \text{ and} \\ \mu_i &= \frac{1}{5}(p^i_{LE} + p^i_{RE} + p^i_N + p^i_{LM} + p^i_{RM}). \end{aligned} \tag{6}$$

Fig. 4(c) shows that the amount of distortion is very small in the central region of the image whereas it increases toward the peripheral region. For this reason, we classify the FLP sets into: i) ideal facial landmark points (IFLPs) in the central region and ii) distorted facial landmark points (DFLPs) in the peripheral region. Among N_F FLP sets, the one with the minimum distance to the center is selected as the IFLP set as

$$L_I = L_{i^*}, \text{ for } i^* = \underset{i \in \{1,\ldots,N_F\}}{\arg\min} \|\mu_i - C\|, \tag{7}$$

where $C = (x_c, y_c)$ is the geometric center of input image.

B. DISTORTION PARAMETER ESTIMATION FOR ITERATIVE CORRECTIONS

In the peripheral region of the image, neighboring pixels become closer to each other as shown in Fig. 4(b), and FLPs are not the exception. Therefore, the standard deviation of a set of FLPs decreases in the peripheral region. Based on this conjecture, the standard deviation of a set of FLPs is a robust measure to determine the amount of distortion.

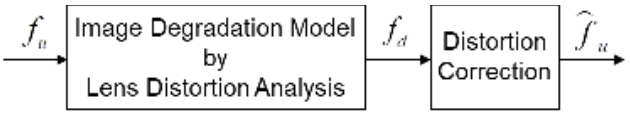

FIGURE 5. Entire process of distorted image acquisition and its correction under the general image correction framework: f_u is an ideal undistorted scene, f_d is the distorted image acquired by a fisheye lens, and $\hat{f}_u$ is an estimated image by correcting the distorted image.

We iteratively estimate the corrected image using the first-order division model in (5). At each iteration we update the corrected image as follows

$$\hat{f}_u^{(j+1)} = \frac{1}{1 + k^{(j)} r^{(j)2}} \hat{f}_u^{(j)}, \text{ for } j = 0, 1, 2, \ldots, N_I, \tag{8}$$

where N_I is the total number of iterations that satisfies a modified convergence condition, which will be given in (13), and the distorted image is used as the initial solution such as $\hat{f}_u^{(0)} = f_d$. At every iteration, $r^{(j)}$ and $k^{(j)}$ are respectively computed as

$$r^{(j)} = \sqrt{\left(\hat{x_u}^{(j)} - \hat{x_c}^{(j)}\right)^2 + \left(\hat{y_u}^{(j)} - \hat{y_c}^{(j)}\right)^2}, \tag{9}$$

where $(\hat{x_u}^{(j)}, \hat{y_u}^{(j)})$ and $(\hat{x_c}^{(j)}, \hat{y_c}^{(j)})$ respectively represent the coordinates of the j-th iterative image point and its center.

The distortion parameter of the j-th iterative image is computed as

$$k^{(j)} = \frac{1}{N_F - 1} \sum_{i \neq i^*} \|\sigma_i^{(j)} - \sigma_{i^*}^{(j)}\|, \tag{10}$$

where σ_{i^*} is the standard deviation of the IFLP, and σ_i are the standard deviations of the DFLP sets.

C. OFF-LINE CORRECTION USING PRE-ESTIMATED PARAMETERS

The proposed distortion correction method has an off-line version as well as the on-line version described in the previous subsection. The off-line version can correct the barrel distortion of a faceless input image using a set of pre-trained distortion parameters. The detail of the off-line version is illustrated in Fig. 1(c). Experimental results of the off-line version will also be given in section V-D.

IV. SELECTION OF THE OPTIMALLY CORRECTED IMAGE

The proposed algorithm can be considered in the general framework of image correction. In other words, the distorted image is considered as a degraded version of the ideal undistorted scene, and the corrected image is an estimation of the ideal scene using the image correction process, which is the distortion correction step in this work. The image correction framework is shown in Fig. 5. Although noise is an important factor that degrades the image quality, the noise power estimation [27] and denoising is out of the scope of this work.

In an ideal case, a corrected image should be the same as the ideal image yielding

$$\|f_u - \hat{f}_u\| = 0. \tag{11}$$

However, (11) is not satisfied in practice because the lens distortion is a spatially variant transformation, which cannot be accurately modeled using a single image degradation operation. Instead of the image subtraction-based error function in (11), we select an optimally corrected image among multiple iterative solutions computed in (8). In the selection process, we use an optical property that is robust to the geometric distortion. More specifically, in the projection process from the 3D world space to the 2D image plane, a straight line bends and becomes a curve by the radial distortion of the lens. In contrast, the correction process should make the curve as straight as possible.

Let $\{\hat{f}_u^{(j)}\}_{j=1}^{N_I}$ be the set of N_I iterative solutions for distortion correction using (8), we select the solution with the fewest number of straight lines as

$$\hat{f}_u^* = \hat{f}_u^{(j^*)}, \text{ where } j^* = \min_{j\in\{1,\ldots,N_I\}} \left|S_j\right|, \tag{12}$$

where S_j represents a set of straight lines extracted in the j-th corrected image, $\hat{f}_u^{(j)}$, and $|\cdot|$ the number of elements in the set.

A curve in a digital image is extracted as multiple line segments whereas a straight line is extracted as a single or a few line segments. Based on this observation, we assume that a corrected image should have a smaller number of line segments than the correspondingly distorted version. To detect line segments, we adopt the distortion-adaptive sobel filter proposed by Frunari *et al.* [28]. Since existing gradient-based line detection methods do not consider a geometric distortion, it is impossible to detect lines in the peripheral region. In this context, the distortion-adaptive sobel filter is suitable for detecting lines in the entire image because it geometrically calculates the gradient using both the distorted and corrected images.

Given the j-th iterative solution, $\hat{f}_u^{(j)}$, we first estimate the gradient image, $\nabla\hat{f}_u^{(j)}$. Line segments are then extracted in the gradient image using the line segment detector (LSD) proposed by von Gioi *et al.* [29]. When we select an optimally corrected image using only the straight line constraint, lines directed toward the distortion center produce an overcorrected result. To prevent the overcorrection problem, the selection method given in (12) is modified as

$$\hat{f}_u^* = \hat{f}_u^{(j^*)}, \text{ where } j^* = \min_j \left(\frac{|S_j|}{D_j} + \sigma_L^{(j)}\right), \tag{13}$$

where D_j is the sum of the lengths of all the line segments in $\hat{f}_u^{(j)}$, $\sigma_L^{(j)}$ is the standard deviation of the FLPs, and $\hat{f}_u^*$ is the final optimally selected correction result image. The finally selected image using (13) can overcome the overcorrection problem by combining the difference in the facial landmark points and the line information.

V. EXPERIMENTAL RESULTS

For the objective assessment of the proposed method, the performance of the proposed method is compared with existing methods. We also proposed a novel evaluation method using optical characteristics of the imaging system. The experiment evaluates the performance of three different methods including: i) calibration pattern-based in subsection V-A, ii) FLP-based in subsection V-B, and iii) off-line, in subsection V-D, correction methods. Subsection V-C analyzes the performance of the FLP-based correction method according to the selected distortion parameters.

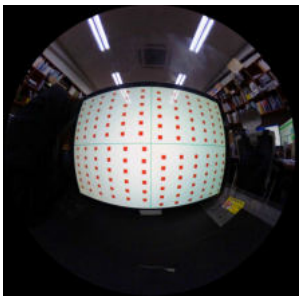

(a)

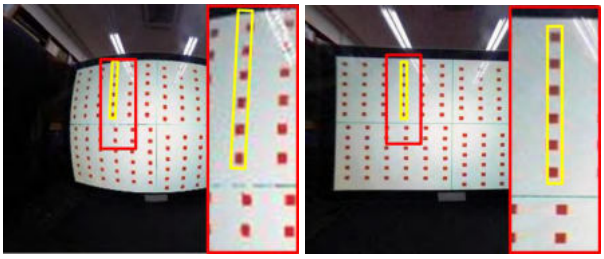

(b) (c)

FIGURE 6. A geometrically distorted image acquired by Samsung Gear 360 camera and correction results using two different methods: (a) input distorted image, (b) corrected image using Kim's method [15], and (c) corrected image using the proposed method.

A. CALIBRATION PATTERN-BASED METHOD

In this section, the performance of the proposed method is compared with results of using calibration pattern. We acquired a set of test images using Samsung Gear 360 camera consisting of two fisheye lens cameras with a FOV of 195°. Fig. 6 shows the comparative experimental results of Kim's calibration pattern-based method [15] and the proposed method. In the experiment, we estimated the distortion parameters using the proposed method to correct a distorted image. As shown in Fig. 6(b), Kim's method produces an inaccurately corrected result because of an insufficient number of calibration pattern points for the distortion ratio estimation. However, the proposed method can correctly remove the distortion in the image. In Figs. 6(b) and 6(c), a region containing vertically aligned points is magnified for comparison.

Fig. 7 demonstrates that the performance of calibration pattern-based method is limited since calibration points exist only near the image center and there is no information for calibration in the peripheral region.For the objective assessment, we proposed *distance ratio*, which is a novel measurement metric to evaluate the performance of correcting the geometric distortion. More specifically, we define three directional

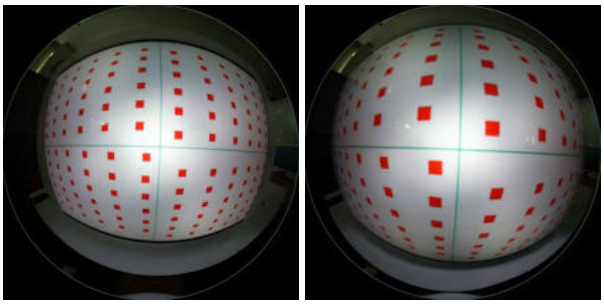

(a) (b)

FIGURE 7. Distorted pattern images acquired by Samsung Gear 360 with different distances between calibration pattern and lens: (a) 2 cm, and (b) 1.5 cm.

TABLE 1. Performance comparison between the calibration pattern-based method and the proposed method using the distance ratio.

	The calibration pattern-based method	The proposed method
ψ_H	1.885	1.372
ψ_V	1.720	1.442
ψ_D	2.963	2.004

distance ratios including horizontal, vertical, and diagonal directions, respectively:

$$\psi_H = \frac{\sum \hat{r}_H}{\sum r_H}, \quad \psi_V = \frac{\sum \hat{r}_V}{\sum r_V}, \text{ and } \psi_D = \frac{\sum \hat{r}_D}{\sum r_D}, \tag{14}$$

where r_H and $\hat{r}_H$ represent the distance between two horizontally adjacent points in the ideal, undistorted image and in the corrected image, respectively. The vertical and diagonal counterparts are also defined in the same manner as shown in Fig. 8. Motivation for the proposed distance ratio is based on the observation that the distance between the dots of the distorted pattern becomes smaller than the ideal calibration pattern.

The distortion correction result consists of three case: i) in the ideal case, the distortion parameter (ψ_H, ψ_V, ψ_D) is close to unity because (r_H, r_V, r_D) and $(\hat{r}_H, \hat{r}_V, \hat{r}_D)$ are same, ii) (ψ_H, ψ_V, ψ_D) is larger than unity because $(\hat{r}_H, \hat{r}_V, \hat{r}_D)$ is larger than (r_H, r_V, r_D) for the barrel distortion, and iii) (ψ_H, ψ_V, ψ_D) is smaller than unity for the pincushion distortion. Table 1 shows the estimated distance ratios from Figs. 6(b) and 6(c). In order to compare the exact distance ratio, we used a front-parallel undistorted image with the same resolution of the distorted image. As shown in Table 1, the proposed method has all three ratios closer to unity than the calibration pattern-based method.

B. FLP-BASED DISTORTION PARAMETER ESTIMATION METHOD

The proposed method uses FLPs of a distorted image to estimate the distortion parameter and then corrects the distortion using the estimated distortion parameter. Fig. 9 shows that the proposed method outperforms the existing methods in both the minimization of overcorrection and the overall subjective

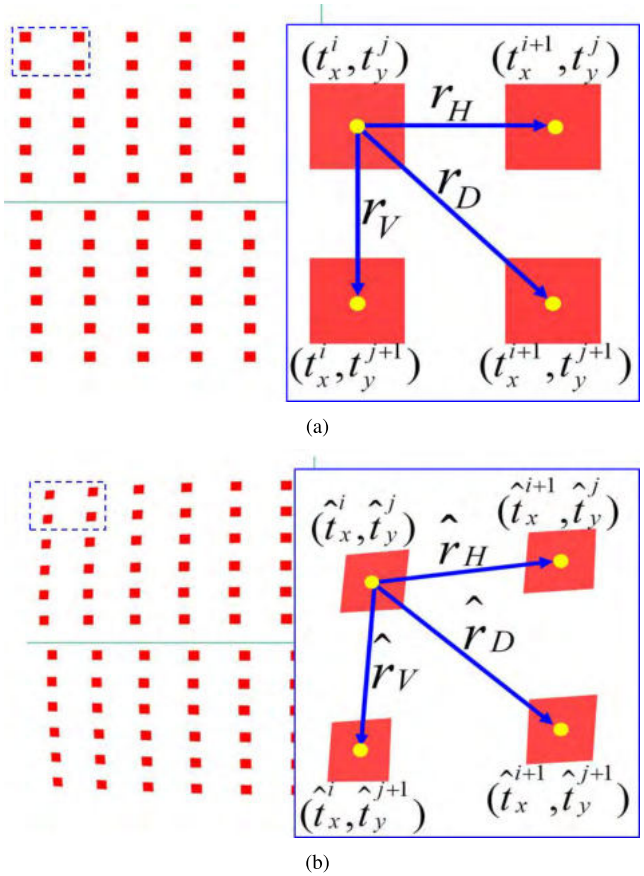

FIGURE 8. Distance gap between the ideal pattern and the distortion correction result with weak distortion: (a) ideal pattern, and (b) distortion correction pattern image.

image quality. More specifically, the first row in Fig. 9 shows the input distorted image and three different correction results using randomly chosen distortion parameters including $k = 0.2$, 0.26, and 0.3. The second row in Fig. 9 shows the correction results of the proposed method, including the optimally corrected result. As shown in Fig. 9(a), the fisheye lens distortion tends to bend a line outward along the radial direction as marked by the red arrows. However, overcorrection makes a line bend inward along the radial direction as shown in Fig. 9(d). It is not easy for existing methods to select the best corrected results among Figs. 9(e)–(h).

The proposed method can automatically correct a distortion by using an appropriately estimated distortion parameter. Moreover, it can avoid the overcorrection problem by selecting the optimally corrected solution using the FLPs and straight line analysis.

C. SELECTION OF THE OPTIMAL DISTORTION PARAMETER

The foundation of the proposed selection method for the optimally corrected result is the characteristics of the fisheye lens that transforms a line into a curve. Figs. 10 and 11 show experimental evidence of our assumption. We chose a brick image to evaluate the number of line segments as shown in Fig. 10(a). If a line bends, the resulting curve is divided

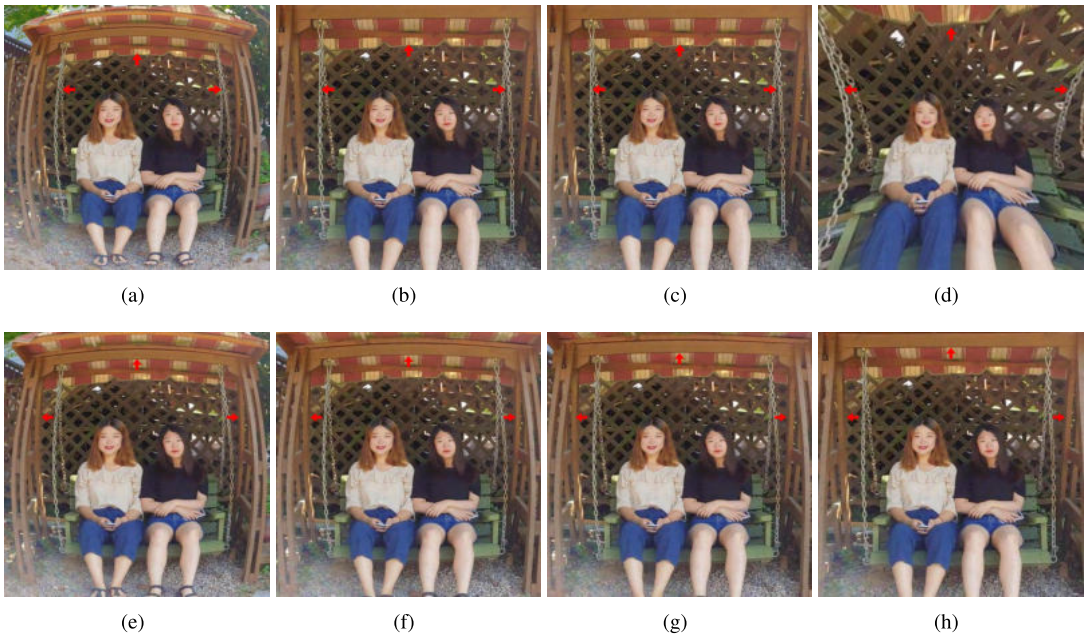

FIGURE 9. Distortion correction results using the division model and the proposed method: (a) input distorted image, (b)–(d) correction results using the division model with distortion parameters $k = 0.2$, $k = 0.26$ and $k = 0.3$, respectively, (e)–(g) correction results using the proposed method with different iterations steps, and (h) the optimally selected result among the different iterations of the proposed method.

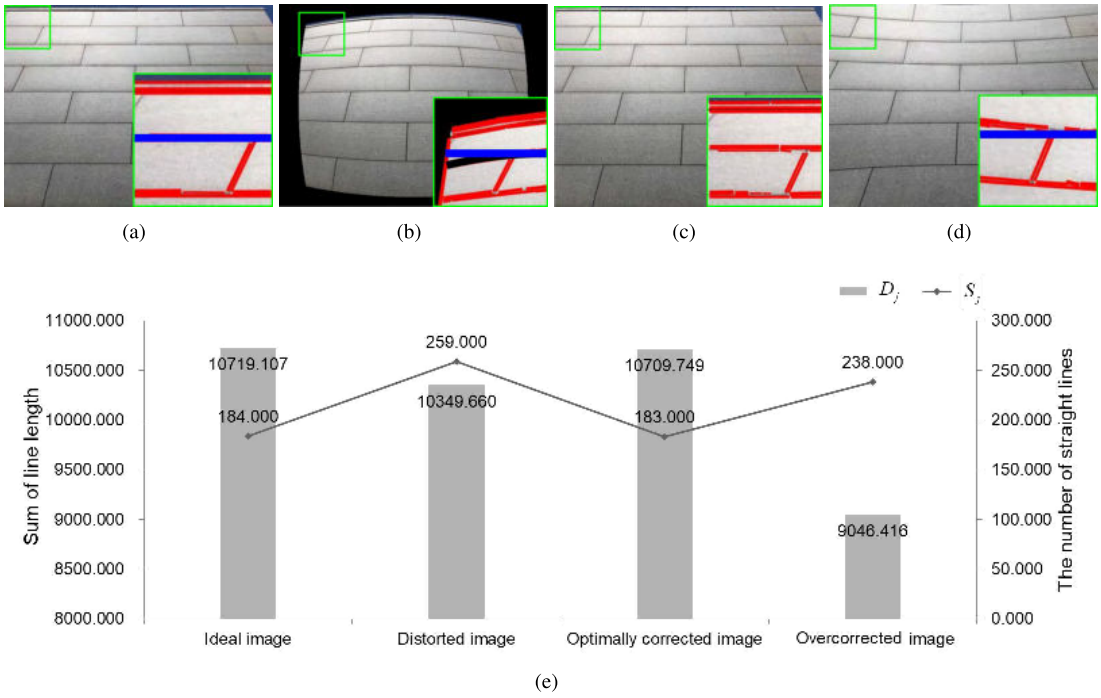

FIGURE 10. Number of line segments in a simulated fisheye lens image and corrected results: (a) ideal image, (b) distorted image, (c) properly corrected image, (d) overcorrected image, and (e) the number of line segments in (a)–(d).

into many small line segments. For that reason, the more the image is distorted, the larger the number of line segments that are produced. As shown in Fig. 10(e), the properly corrected image has fewer line segments than both the distorted and the overcorrected images.

Fig. 11 shows the proposed iterative distortion correction results in the first row and the number of line segments and their average lengths for each iteration in the second row. After each iteration, we crop the central region of the image with the ratio 4:1 and make the best view of distortion corrected result. Fig. 11(b) shows the visually best view of corrected result selected by the proposed method. Figs. 11(c) and 11(d) respectively show the number of extracted lines and scores estimated by (13) versus the

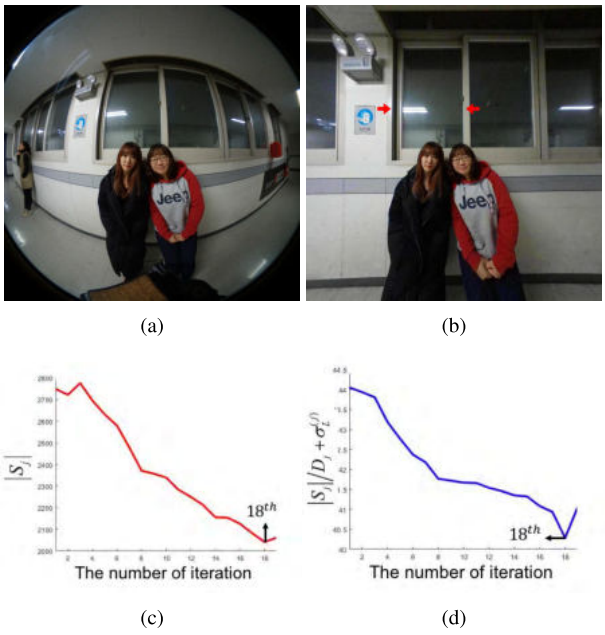

FIGURE 11. The number of line segments and the modified scores given in (13): (a) input distorted image, (b) the optimally corrected image, (c) the number of lines versus iteration, and (d) the modified scores versus iteration.

iteration step, respectively. As shown in Fig. 11, the minimum of both number of straight lines and scores appear at the 18-th iteration.

Because the line information is a dominant factor in selecting the optimally corrected image, the selection of an appropriate line detection method is important. Although Benligiray *et al*. recently proposed a line detection method to correct the geometric distortion [20], they detected only collinear lines in the real world. For this reason, the accuracy of Benligiray's method depends on the number of collinear lines in the central and peripheral regions of the image. To overcome this limitation, we detected all the straight lines using the distortion-adaptive sobel filter. Fig. 12 shows the line detection results using Benligiray's and the proposed methods. As shown in Fig. 12, the proposed method detected more lines than Benligiray's method. The proposed method can successfully make bent lines (or curves) in a distorted image straight, whereas Benligiray's method cannot.

The proposed method is compared with Cho's method [18] to evaluate the accuracy of the distortion correction. Cho's method uses the FLPs to correct the lens distortion, whereas the proposed method employs two features, FLPs and line segments. For the subjective and objective evaluation of both results, we propose a novel numerical distortion measurement method. The foundation of the proposed numerical measurement is that the straight line in the 3D real world has to be straight in an undistorted image based on the optical projection theorem. Devernay's [30] method uses the transformed information of the straight line detected in the image. On the other hand, the proposed method selects the optimally corrected image using the number and total length of all the line segments.

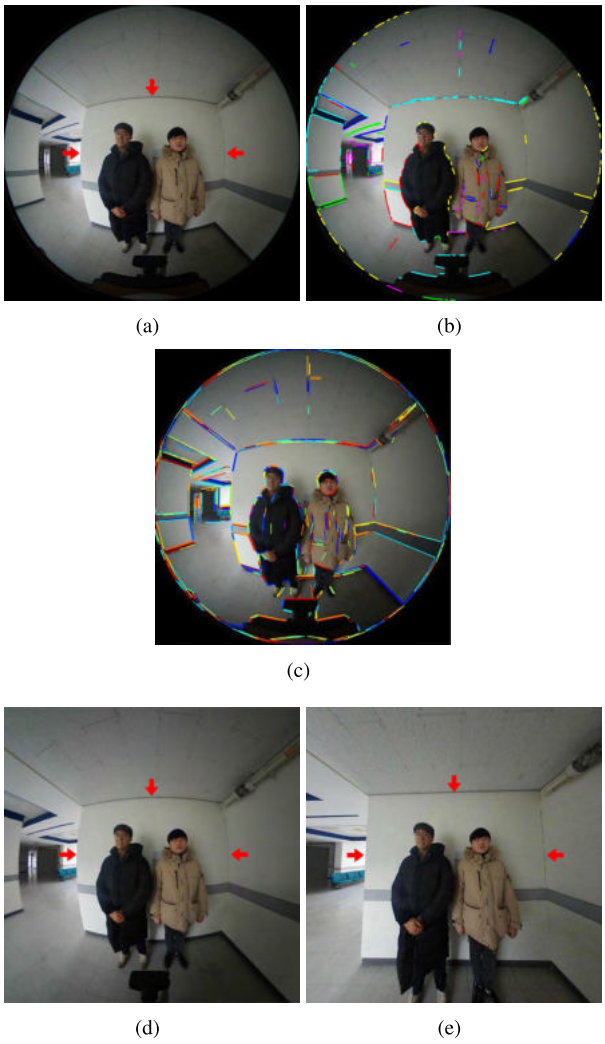

FIGURE 12. Line detection and distortion correction results using Benligiray's [20] and the proposed methods: (a) input distorted image, (b) line detection result using Benligiray's method, (c) line detection result using the proposed method using the distortion-adaptive sobel filter, (d) correction result using Benligiray's method, and (e) correction result using the proposed method. (Best viewed in color.)

As shown in Fig. 13, the proposed method completely removed the distortion artifact. However, in the result of Cho's method, the distortion remains at the joint of the ceiling and the wall indicated by a red arrow. Cho's method cannot accurately correct the distortion because the FLPs are located in the central region where the standard deviation of the FLPs is continuously reduced during the iterations. Hence, the iterative distortion correction process is terminated because Cho's method uses the standard deviation as a termination condition.

Fig. 14 shows a pair of undistorted and distorted images. A straight line in the undistorted image is transformed into an arc in the distorted image. Each arc is characterized by two lines as shown in Fig. 14, and their relationship is determined as the distortion ratio, denoted as R_D

$$R_D = \left(1 - \frac{L+\gamma}{2H}\right) \times 100, \tag{15}$$

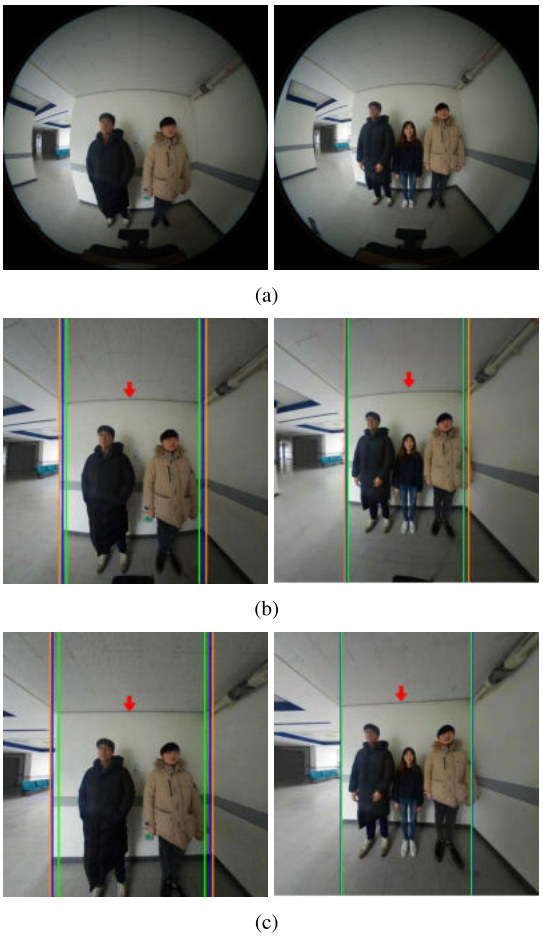

FIGURE 13. Comparative experimental results: (a) input distorted images, (b) correction results using Cho's method, and (c) correction results using the proposed method.

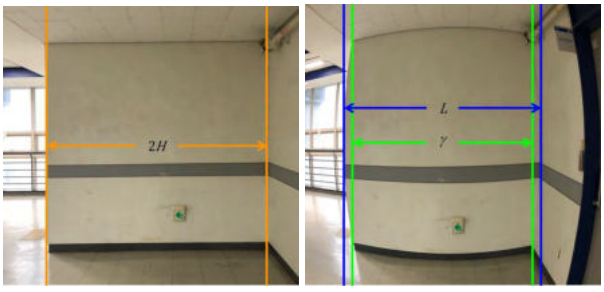

FIGURE 14. Analysis of straight lines: (a) straight lines in the ideal, undistorted image, and (b) tangent lines of arcs in the distorted image.

where H is the distance between the right end and left walls in the ideal image, and L and γ respectively represent the maximum and minimum distances between the walls in the distorted image. In the distortion-free image, $2H$ is equals to $L+\gamma$, and the distortion ratio R_D becomes zero.

Table 2 compares the distortion ratio of the corrected results using Cho's and the proposed methods as shown in Fig. 13. The distortion ratio of the proposed method is smaller than Cho's method. The second test image has a lower distortion ratio than the first image because of different tilting angles of the camera.

TABLE 2. Distortion ratio comparison of Fig. 13.

	Cho's method (%)	The proposed method (%)
Left column	7.485	6.492
Right column	5.873	1.157

TABLE 3. Conventions.

C	center of image, $C=(x_c, y_c)$
D_j	sum of the lengths of all line segments in $\hat{f}_u^{(j)}$
L_i	i-th set of five Facial landmark points (FLP), $L_i=\{p^i_{LE}, p^i_{LRE}, p^i_N, p^i_{LM}, p^i_{RM}\}$
L_I	ideal FLP set with minimum distance from FLP to the center
$L(\cdot)$	function of the Division model
N_I	final number of iterations
P	A point in the three-dimensional coordinate, $P=(X,Y,Z)$
R_D	distance ratio according to the L, λ, and H
S_j	set of straight lines extracted in the j-th iterative correction
$FLPs$	Facial landmark points
$IFLPs$	Ideal facial landmark points ($IFLPs$) in the central region from FLP set
$DFLPs$	Distorted facial landmark points ($DFLPs$), the value except for $IFLP$ in FLP set
f_d	the input distorted image
f_u	the ideal undistorted image
$\hat{f}_u$	an estimated correction result
$\nabla\hat{f}_u^{(j)}$	gradient image of j-th iterative estimation result
$\hat{f}_u^*$	optimally selected correction result
$k^{(j)}$	the estimated distortion parameter of j-th iterations
p	A point in the two-dimensional coordinate, $p=(x,y)$
p_u	A point in an undistorted image, $p_u=(x_u, y_u)$
p_d	A point in a distorted image, $p_d=(x_d, y_d)$
p^i_F	coordinates of five FLP: left eye(LE), right eye(RE), nose(N), left corner of mouth(LM), right corner of mouth(RM), $F\in\{LE, RE, N, LM, RM\}$
$r^{(j)}$	distance between the center and the point in j-th corrected image
ψ_H	distance ratio in the horizontal direction
ψ_V	distance ratio in the vertical direction
ψ_D	distance ratio in the diagonal direction
$\lvert\cdot\rvert$	number of elements in the set
μ_i	the mean of the set of FLPs for i-th iterations, $i=1,\ldots,N_F$
$\sigma_L^{(j)}$	the standard deviation of the set of FLPs for j-th iterations

D. OFF-LINE CORRECTION METHOD

The last experiment is performed to verify that the proposed method can be applied to various practical applications. Test images without human faces are acquired from the real-world scene containing multiple objects at different distances. If the input image does not contain faces, the off-line version of correction is performed using the pre-estimated distortion parameters that were obtained from the on-line correction of the same camera as shown in Fig. 13. The results of this experiment are shown in Fig. 15(b), which demonstrates that the proposed method successfully corrects the geometric distortion without depth parallax artifacts. The on-line version of the correction algorithm takes a geometrically distorted image containing human faces to estimate the distortion parameter. On the other hand, the off-line version first calibrates the same camera using facial images prior to the main

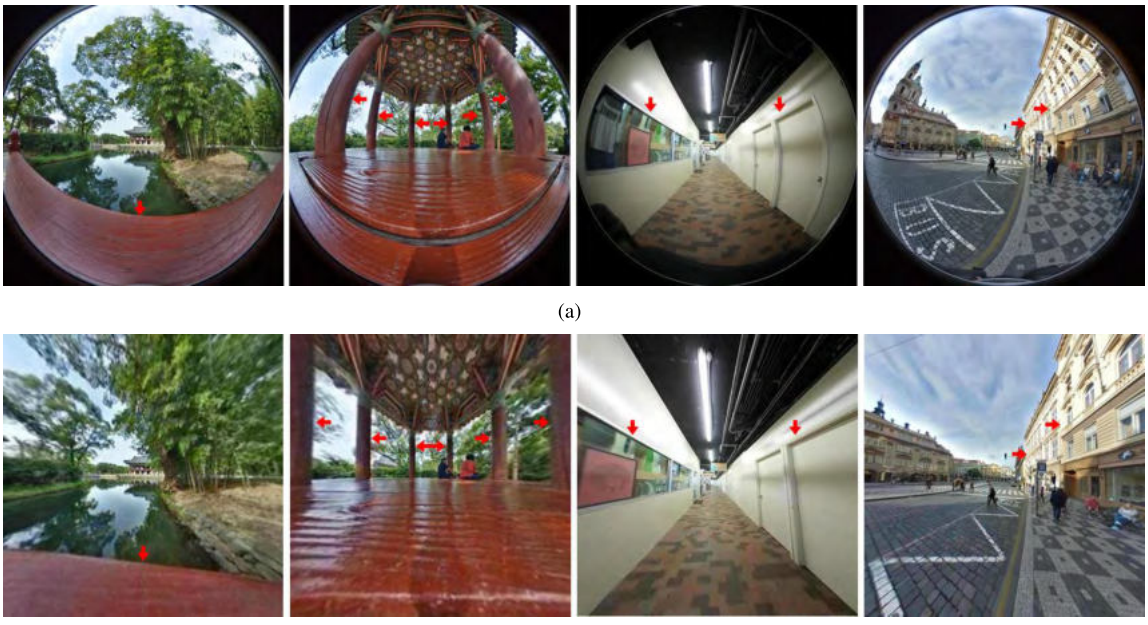

(a)

(b)

FIGURE 15. Correction results of distorted images with various acquisition conditions and places: (a) input distorted images and (b) distortion correction results of (a).

processing, and then performs correction on the faceless input image using the estimated distortion parameter. Table 3 shows the notation conventions. When the input image does not have a sufficient amount of illumination, a pre-processing to enhance the contrast [31] can increase the accuracy of distortion parameter estimation.

VI. CONCLUSIONS

We presented an automatic image-based method to correct a barrel distortion in fisheye lens images. Despite an unparalleled advantage of wide field-of-view, the practical application of a fisheye lens camera is limited because of the nonlinear distortion in the acquired image and complicated preprocessing steps to correct the distortion.

The proposed correction method requires neither *a priori* lens design specifications nor a special calibration pattern to estimate the distortion parameter. It first extracts facial features using a set of image processing algorithms to estimate the distortion parameter. Given the parameter, the iterative procedure generates multiple differently corrected solutions, and then the optimally corrected solution is selected by analyzing the line segments in the image. An additional, but practically very useful, the contribution of the proposed work is to provide both on-line and off-line correction processes depending on the existence of facial features in the scene.

Since the proposed method consists of only image processing algorithms, it can make wide field-of-view imaging systems applicable to extended application fields, including 360° AR or VR cameras, wide-area surveillance systems.

REFERENCES

[1] R. Hill, "A lens for whole sky photographs," *Quart. J. Roy. Meteorol. Soc.*, vol. 50, no. 211, pp. 227–235, 1924.

[2] J. J. Kumler and M. L. Bauer, "Fish-eye lens designs and their relative performance," *Proc. SPIE*, vol. 4093, pp. 360–370, Oct. 2000.

[3] D. Tseng, C. Chen, and C. Tseng, "Automatic detection and tracking in multi-fisheye cameras surveillance system," *Int. J. Comput. Elect. Eng.*, vol. 9, 2017.

[4] G. Klein and D. W. Murray, "Simulating low-cost cameras for augmented reality compositing," *IEEE Trans. Vis. Comput. Graphics*, vol. 16, no. 3, pp. 369–380, May 2010.

[5] H. Luo, T.-S. Pan, J.-S. Pan, S.-C. Chu, and B. Yang, "Development of a three-dimensional multimode visual immersive system with applications in telepresence," *IEEE Syst. J.*, vol. 11, no. 4, pp. 2818–2828, Dec. 2017.

[6] J. Hernandez-Vicen, S. Martinez, J. M. Garcia-Haro, and C. Balaguer, "Correction of visual perception based on neuro-fuzzy learning for the humanoid robot TEO," *Sensors*, vol. 18, no. 4, p. 972, 2018.

[7] C. Hughes, M. Glavin, E. Jones, and P. Denny, "Wide-angle camera technology for automotive applications: A review," *IET Intell. Transp. Syst.*, vol. 3, no. 1, pp. 19–31, Mar. 2009.

[8] R. Y. Tsai, "A versatile camera calibration technique for high-accuracy 3D machine vision metrology using off-the-shelf TV cameras and lenses," *IEEE J. Robot. Autom.*, vol. RA-3, no. 4, pp. 323–344, Aug. 1987.

[9] J. Mallon and P. F. Whelan, "Precise radial un-distortion of images," in *Proc. 17th Int. Conf. Pattern Recognit.*, vol. 1, 2004, pp. 18–21.

[10] H. Ojanen, "Automatic correction of lens distortion by using digital image processing," Dept. Math., Rutgers Univ., Tech. Rep., 1999.

[11] G. Vass and T. Perlak, "Applying and removing lens distortion in post production," in *Proc. 2nd Hungrian Conf. Comput. Graph. Geometry*, 2003, pp. 9–16.

[12] C. Brauer-Burchardt and K. Voss, "A new algorithm to correct fish-eye- and strong wide-angle-lens-distortion from single images," in *Proc. Int. Conf. Image Process.*, vol. 1, 2001, pp. 225–228.

[13] C. Hughes, P. Denny, E. Jones, and M. Glavin, "Accuracy of fish-eye lens models," *Appl. Opt.*, vol. 49, no. 17, pp. 3338–3347, Jun. 2010.

[14] J. Park, S.-C. Byun, and B.-U. Lee, "Lens distortion correction using ideal image coordinates," *IEEE Trans. Consum. Electron.*, vol. 55, no. 3, pp. 987–991, Aug. 2009.

[15] H. Kim, D. Kim, and J. Paik, "Automatic estimation of spatially varying focal length for correcting distortion in fisheye lens images," *IEIE Trans. Smart Process. Comput.*, vol. 2, no. 6, pp. 339–344, 2013.

[16] Y. Wu, S. Jiang, Z. Xu, S. Zhu, and D. Cao, "Lens distortion correction based on one chessboard pattern image," *Frontiers Optoelectron.*, vol. 8, no. 3, pp. 319–328, 2015.

[17] T.-Y. Lee, T.-S. Chang, and S.-H. Lai, "Correcting radial and perspective distortion by using face shape information," in *Proc. 11th IEEE Int. Conf. Workshops Autom. Face Gesture Recognit. (FG)*, vol. 1, May 2015, pp. 1–8.
[18] W. Cho, M. Lee, H. Kim, and J. Paik, "Automatic estimation of distortion coefficient for correcting radial distortion," in *Proc. Int. Conf. Electron., Inf., Commun. (ICEIC)*, 2018, pp. 1–3.
[19] D. Claus and A. W. Fitzgibbon, "A rational function lens distortion model for general cameras," in *Proc. IEEE Comput. Soc. Conf. Comput. Vis. Pattern Recognit.*, vol. 1, pp. 213–219, 2005.
[20] B. Benligiray and C. Topal, "Blind rectification of radial distortion by line straightness," in *Proc. 24th Eur. Signal Process. Conf. (EUSIPCO)*, 2016, pp. 938–942.
[21] D. Santana-Cedrés *et al.*, "Estimation of the lens distortion model by minimizing a line reprojection error," *IEEE Sensors J.*, vol. 17, no. 9, pp. 2848–2855, May 2017.
[22] M. Alemán-Flores, L. Alvarez, L. Gomez, and D. Santana-Cedrés, "Automatic lens distortion correction using one-parameter division models," *Image Process. On Line*, vol. 4, pp. 327–343, Nov. 2014.
[23] C. Cho, N. I. Park, B. Kim, Y. Lee, and I. H. Yoon, "Information gain-based initialization for stable topological derivative segmentation," *TECHART, J. Arts Imag. Sci.*, vol. 5, no. 3, pp. 32–37, 2018.
[24] B. Adithya, L. Hanna, P. Kumar, and Y. Chai, "Calibration techniques and gaze accuracy estimation in pupil labs eye tracker," *TECHART, J. Arts Imag. Sci.*, vol. 5, no. 1, pp. 38–41, 2018.
[25] S. Milborrow and F. Nicolls, "Locating facial features with an extended active shape model," in *Proc. Eur. Conf. Comput. Vis. (ECCV)*, 2008, pp. 504–513.
[26] K. Zhang, Z. Zhang, Z. Li, and Y. Qiao, "Joint face detection and alignment using multitask cascaded convolutional networks," *IEEE Signal Process. Lett.*, vol. 23, no. 10, pp. 1499–1503, Oct. 2016.
[27] Y. Yoo, J. Shin, and J. Paik, "Minimum statistics-based noise power estimation for parametric image restoration," *IEIE Trans. Smart Process. Comput.*, vol. 3, pp. 41–51, Apr. 2014.
[28] A. Furnari, G. M. Farinella, A. R. Bruna, and S. Battiato, "Distortion adaptive Sobel filters for the gradient estimation of wide angle images," *J. Vis. Commun. Image Represent.*, vol. 46, pp. 165–175, Jul. 2017.
[29] R. G. von Gioi, J. Jakubowicz, J.-M. Morel, and G. Randall, "LSD: A line segment detector," *Image Process. On Line*, vol. 2, pp. 35–55, Mar. 2012.
[30] F. Devernay and O. Faugeras, "Straight lines have to be straight," *Mach. Vis. Appl.*, vol. 13, no. 1, pp. 14–24, 2001.
[31] J. Shin, H. Park, J. Park, J. Paik, and J. Ha, "Variational low-light image enhancement based on a haze model," *IEIE Trans. Smart Process. Comput.*, vol. 7, no. 4, pp. 325–331, 2018.

MINJUNG LEE was born in Busan, South Korea, in 1994. She received the B.S. degree in electronics engineering from Silla University, in 2017, and the M.S degree in image engineering from Chung-Ang University, Seoul, in 2019, where she is currently pursuing the Ph.D. degree in image engineering

Her research interests include geometric distortion correction, object parsing, and feature extraction.

HYUNGTAE KIM (S'14) was born in Seoul, South Korea, in 1986. He received the B.S. degree from the Department of Electrical Engineering from Suwon University, in 2012, and the M.S degree in image engineering from Chung-Ang University, in 2015, where he is currently pursuing the Ph.D. degree in image engineering.

His research interest includes multicamera calibration based on large-scale video analysis.

JOONKI PAIK (M'89–SM'12) was born in Seoul, South Korea, in 1960. He received the B.Sc. degree in control and instrumentation engineering from Seoul National University, in 1984, and the M.Sc. and Ph.D. degrees in electrical engineering and computer science from Northwestern University, in 1987 and 1990, respectively. From 1990 to 1993, he joined Samsung Electronics, where he designed image stabilization chipsets for consumer camcorders. Since 1993, he has been a member of the faculty with Chung-Ang University, Seoul, where he is currently a Professor with the Graduate School of Advanced Imaging Science, Multimedia, and Film. From 1999 to 2002, he was a Visiting Professor with the Department of Electrical and Computer Engineering, The University of Tennessee, Knoxville. Since 2005, he has been the Head of the National Research Laboratory in the field of image processing and intelligent systems. From 2005 to 2007, he served as the Dean of the Graduate School of Advanced Imaging Science, Multimedia, and Film. From 2005 to 2007, he was the Director of the Seoul Future Contents Convergence Cluster established by the Seoul Research and Business Development Program. In 2008, he was a full-time Technical Consultant for the System LSI Division of Samsung Electronics, where he developed various computational photographic techniques, including an extended depth of field system. He is currently serving as a member of the Presidential Advisory Board for Scientific/Technical Policy with the Korean Government and a Technical Consultant for the Korean Supreme Prosecutor's Office for computational forensics. He was a recipient of the Chester-Sall Award from the IEEE Consumer Electronics Society, the Academic Award from the Institute of Electronic Engineers of Korea, and the Best Research Professor Award from Chung-Ang University. He has served the Consumer Electronics Society of the IEEE as a member of the Editorial Board.